Determination of Stress Intensity
Factor Distributions For "Interface"
Cracks in Incompressible, Dissimilar Materials

SUMMARY REPORT

C.W. Smith, P.I.

Reporting Period - 8/15/94 - 12/31/97

Grant No. NAG-1-1622-Supl. 1-5*

Office of Sponsored Programs
301 Burruss Hall
Virginia Polytechnic Institute and State University
Blacksburg, VA 24061

INTRODUCTION

The present study was undertaken in order to develop test methods and procedures for measuring the variation of the stress intensity factor through the thickness in bimaterial specimens containing cracks within and parallel to the bond line using the frozen stress photoelastic method. Since stress freezing materials are incompressible above critical temperature, and since thick plates are to be employed which tend to produce a state of plane strain near the crack tip, the interface near tip fracture equations [1] reduce to the classic form for homogeneous materials. Moreover, zero thickness interfaces do not exist when materials are bonded together.

It was decided early on that it would be important to insure a uniform straight and accurate crack tip region through the thickness of the body to reduce scatter in the SIF distribution through the thickness. It was also observed that rubberlike materials which were desired to be modeled exhibited significant tip blunting prior to crack extension and that some blunting of the tip would provide a more realistic model. It should be noted that, in normal stress freezing photoelastic work, it is considered good practice to avoid utilizing data near bond lines in photoelastic models due to the bond line stresses which inevitably develop when two parts are bonded together. Thus, the present study involves certain exploratory aspects in deviating from standard practice in stress freezing work.

With the above ideas in mind, several different test methods were investigated and are described in the following sections and appendices. The geometry selected for the program was a thick, edge cracked specimen containing a bond line.

TEST METHODS AND PROCEDURES

Ideally suited materials for the proposed program would be two stress freezing materials with identical thermal coefficients of expansion at both room and critical temperature (T_c) and identical T_c values; in fact, materials identical in all respects except in modulus above T_c. It was found early on that different materials with matching T_c values could not be

2

found, that T_c values (where the material, upon cooling, transforms from the rubbery to the glassy state) even varied for the same material from batch to batch. These limitations led to the investigation of a variety of crack types and material combinations in seeking a reliable combination. All of the frozen stress data were analyzed by the two parameter method developed by the P.I. [2].

A-<u>Bond Line Cracks</u>

The first set of experiments examined two different specimen types for bond line cracks Type A - Two different commercial photoelastic materials with T_c values differing by 20° to 25° F and with matched thermal coefficients of expansion. The crack was formed by placing a thin strip of Teflon over part of the surface to be bonded. Although reasonable results were obtained, replication of specimens was difficult, the crack fronts were not uniform and the bond line thickness could not be kept constant.

Type B - Specimens consisting of pure araldite on one side of the bond line and araldite with 25% by weight of aluminum powder on the other side were used. Here T_c's were matched exactly but the coefficients of thermal expansion above T_c differed by nearly 20%. Cracks were machined in as vee-notches. Again test results were within conventional photoelastic results ($< \pm 4\%$) but the araldite exhibited certain unstable characteristics when thermally cycled repeatedly.

Results from the first set of experiments are presented in [3]. (Appendix I, p. 2, Table III) The Type B experiments used a three specimen test procedure consisting of homogeneous, homogeneous bonded and bimaterial bonded specimens in order to separate out the effect of bond stress from that of modulus mismatch. Results from these experiments are presented in Appendix I, p. 3, Table IV. Then, using the Type B three specimen concept, a series of experiments were conducted for cracks in bond lines inclined to the applied load producing mixed mode local fields as well as pure mode I and results are found in Ref. [4] (Appendix II, p. 4, Table II)). These results revealed that increases in the stress intensity level for the

3

bond line cracks was of the order of 20% above those in a homogeneous specimen for Mode I ($\beta = 0$) and small angles of inclination of the bond line to a normal to the applied load (i.e. $\beta = 15°$). However for larger angles of inclination of 30° and 45°, no increase in the stress intensity level was observed. This was due to the reorientation of the stress fringes relative to the applied load (Ap II, p. 6, Fig. 5). It was also noted that a modulus ratio of 1.98 in the bimaterial specimens had no significant effect on the stress intensity level at the crack tip for $\beta = 0°$. This was also noted in [1]. In all cases, the stress intensity factor (SIF) at mid thickness was always higher than near the edges but the difference was sometimes of the order of the experimental scatter. However, the effect of the homogeneous bond line and bimaterial bond line specimens on the SIF distribution through the thickness did not appear significant.

B-Cracks Parallel to But Not In Bond Line

For this study, edge cracked specimens were again employed and blunted crack tips were machined in to simulate the blunting in the real material. The three specimen method was again employed, and two commercially available stress freezing materials were used. The T_c values differed by 25°F and, in order to minimize this effect, the cracks were located in the material with the highest T_c. In this way, when the higher T_c material became glassy, it was restrained by only the soft part of the bimaterial specimen. (i.e. $E_{soft}/E_{glassy} \approx 0.5\%$). Then, when the lower T_c material became glassy, it only slightly stressed the higher T_c material and this stress was released upon slicing. The effect of this procedure was checked by conducting a no-load stress freezing cycle prior to stress freezing under load. Results (Appendix III, p. 6, Fig. 2, p. 7, Fig.4) showed that only the non-singular stress changed in the data zone and here the change was constant for all data points indicating no resulting effect upon the SIF values. Cracks located 12.7 mm. from the bond line were unaffected by bond stresses in either the homogeneous bonded or the bimaterial bonded specimens. In fact, only the crack 3.18 mm from the bond line in the bonded bimaterial specimen ($E_1/E_2 \approx 4.00$) showed any significant increase in stress intensity level and that increase

was 29%. However, a small shear mode was detected in all cracks not in the bond line (Appendix III p. 7 Fig. 5). Followup experiments using the materials of Appendix II and duplicating this test geometry showed neither shear mode nor SIF elevation suggesting that both of those effects are related solely to T_c mismatch. The SIF distribution through the thickness was thumbnailed as expected and the mid- thickness value varied from 12 to 26% above the edge slice values in the homogeneous specimen and from 6 to 28% in the bimaterial specimens. The results of this part of the study are found in Ref. [5] (Appendix III, p. 3, Table II, Table III).

SUMMARY

By utilizing the three specimen method, frozen stress studies can be used successfully to measure the SIF distribution through the thickness of cracks within and parallel to bond lines, separating bond line residual stresses from modulus and T_c mismatch effects.

The most important finding of this study is that all of the increases in the SIF observed were due to bond line residual stress. Modulus mismatch produced no SIF increases and no shear mode for cracks within or parallel to the bond line. This is not surprising for cracks in thick incompressible materials as noted in Reference [1].

The second most important finding is that most stress freezing materials are not stable enough for tests such as these unless thoroughly post cured and aged for at least six months. Although thermal cycling helps, the age time is still recommended.

Moreover, when using materials with different T_c values, accurate Mode I SIF values can only be obtained for cracks not near the bond line. However, if the crack is within the bond line, the T_c effect will be negligible.

ACKNOWLEDGMENTS

REFERENCES

[1] Hutchinson, J.W. and Suo, Z., "Mixed Mode Cracking in Layered Materials," *Advances in Applied Mechanics* V29 <u>Academic Press</u> p. 63-191, 1992.

[2] Smith, C.W., "Experimental Determination of Stress Intensity Factor Distribution in Engineering Problems," *Applied Mechanics Reviews*, Vol. 46, n11, pt 2, Nov. 1993.

[3] Smith, C.W., Finlayson, E.F. and Liu, C.T., "Preliminary Studies of Three Dimensional Effects on Artificial Cracks at Simulated Rocket Motor Liners by the Frozen Stress Method" *Proceedings of VIII International Congress on Experimental Mechanics* p. 55-61, 1996 (Appendix I of this study)

[4] Smith, C.W., Finlayson, E.F. and Liu, C.T., "A Method for Evaluating Stress Intensity Distribution for Cracks in Rocket Motor Bond Lines" *Journal of Engineering Fracture Mechanics* V58 n1, 2p 97-105, 1997 (Appendix II of this study).

[5] Smith, C.W., Finlayson, E.F. and Liu, C.T., "Bond Line Residual Stress Effects on Cracks Parallel to the Bond Lines in Rubberlike Materials," *Recent Advances in Solids and Structures* ASME PVP V 369 p. 1-9, Nov. 1997 (Appendix III of this study).

Preliminary Studies of Three Dimensional Effects
on Artificial Cracks at Simulated Rocket Moter Liners
by the Frozen Stress Method

C. W. Smith[a], E. F. Finlayson[a] and C. T. Liu[b]

[a]Department of Engineering Science and Mechanics, Virginia Polytechnic Institute and State University,
Blacksburg, VA 24061; [b]OL/AC/PL/RKS, 4 Draco Drive, Edwards Air Force Base, CA 93524-7160

ABSTRACT

In a preliminary study limited to stress freezing materials, two types of bimaterial specimens, one consisting of two photoelastic materials with different critical temperatures (Type A) and one consisting of a photoelastic material with and without aluminum powder (the powder added to alter the modulus of elasticity without changing the critical temperature (Type B)) are constructed by bonding two halves of the dissimilar materials together. Each type of specimen contains an artificial edge crack along the bond line and loaded normal to the bond line. After evaluating the two specimen types by measuring the variation of the Mode I stress intensity distribution through the specimen thickness, Type B was selected as a superior model and its features studied in detail.

INTRODUCTION

When a crack is located at the interface between two materials, near tip stress analysis is complicated by the fact that the mode 1 and mode 2 stress intensity factors (SIF) cannot be decoupled [1]. However, if the materials are incompressible, and plane strain exists, the near tip interface equations reduce to the more familiar form for isotropic and homogeneous elastic solids [2].

When cracks occur between a solid rocket motor and its rubber liner, the above conditions are approximately realized and occur at a rather low modulus ratio between the two materials. The first author and his colleagues have had considerable success in measuring three dimensional effects in cracked isotropic and homogeneous bodies using a refined frozen stress method [3]. The frozen stress method is briefly summarized in Appendix L. In order to explore the feasibility of such an approach in measuring three dimensional and residual stress effects in such cracks as described above, a series of experiments were conducted on thick plates in tension containing bondline cracks between two different incompressible materials. Two specimen types were investigated:

Type A - Two commercially available photoelastic materials with the crack along the bondline created by maintaining material separation with a strip of teflon which was later removed. The specimen geometry is specified in Fig. 1 and pertinent material properties

are given in Table I where f_r is the material fringe value.

Table I

Material	$T_{critical}$	E_{Hot}	f_r
PSM-9	160°F	19.31 MPa	325.7 Pa-m
PLM-4B	140°F	7.65 MPa	262.7 Pa-m

The thermal coefficients of the two materials were given as 39×10^{-6} per °F at room temperature (T_R) and 90×10^{-6} per °F at critical temperature (T_c). The bonding agent is PLM-9, which is an epoxy glue chemically similar to PSM-9.

Type B - Pure araldite was used on one side of the bondline and araldite with 25% by weight of aluminum powder was used on the other side of the bondline to increase the elastic modulus. The thermal coefficients were 15.5×10^{-6} per °F at room temperature and averaged 120×10^{-6} per °F at the T_c with a scatter of $\pm 20 \times 10^{-6}$ per °F. After bonding, a machined
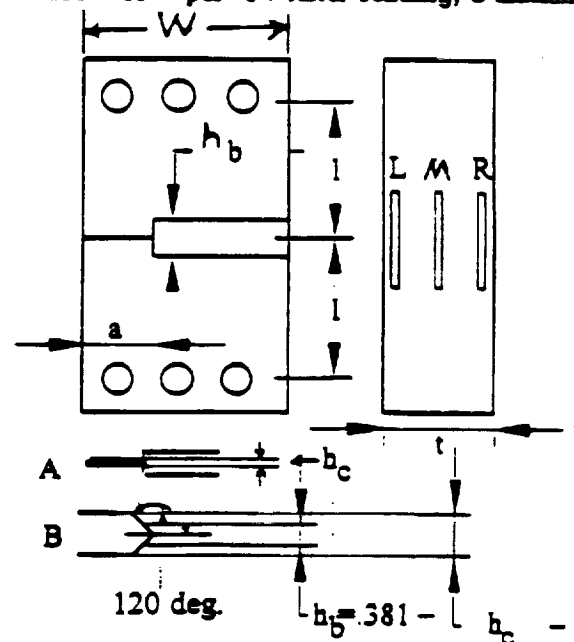
	a	W	l	h_c	t
Type A	12.29	50.80	88.90	.0965	12.70
Type B	9.525	38.10	88.90	1.590	12.70

Dimensions in millimeters

Fig. 1. Test Specimen Dimensions

notch was inserted along the bondline. The pertinent material properties are given in Table II.

Table II

Material	$T_{critical}$	E_{Hot}	f_r
Araldite	280°F	9.44 MPa	266.2 Pa-m
Aral-Alum	280°F	20.06 MPa	_____

PLM-9 epoxy was used as the bonding agent. A machined notch was used to simulate the crack. Its dimensions and those of the test specimens are given in Fig. 1.

Both types of specimens exhibited a residual stress field due to curing of the glue which could not be annealed out because of the constraining effects and in Type A, T_c mismatch also contributed a frozen stress part. Fringe patterns from A and B after stress freezing before and after slicing were used for analysis. A Mode I algorithm for homogeneous material was used to convert the optical data into stress intensity factor (SIF) data. The basic relation and it's use is developed in Appendix II.

TEST RESULTS AND DISCUSSION

Type A - This type of specimen exhibited a residual fringe field mainly due to the mismatch in T_c values but also partially due to shrinkage of the glue. This field, which was retained throughout the stress freezing process, was not symmetrical with respect to the bond line and yielded different values of K_1 on the two sides of the crack. However, when averaged, both the through thickness and slices L, M and R agreed closely with the theoretical value of K_1 provided by [4], as shown in Table III. Unfortunately, however, the teflon strip did not produce a straight crack front free of near tip

Table III (K_1 in MPa$\sqrt{m}$ x 10^3)

Material	Th^a	TT^b	Slice L	Slice M	Slice R
PLM-4B	15.17	14.95	13.18	13.05	13.75
PSM-9	15.17	15.17	15.96	15.44	16.53^c
AVG	15.17	15.06	14.56^d	14.24	15.14^d

^{a} TH = Theoretical result [4];

^{b} TT = Through thickness;

^{c} Estimated from values of L slices;

^{d} LR AVG = 14.85

distortions which caused some data to be erroneous, producing large scatter in K_{AP} vs. $\sqrt{r/a}$ graphs locally. All slices were of the order of 0.89 mm thick and were oriented mutually orthogonal to the crack front and its plane.

In Table III, the difference between the TT result and Th may be attributed to thicknesswise variations

in the SIF which appear to be small. Differences in SIF values on the two sides of the crack in the slices may be attributed to the stress frozen field produced by the T_c mismatch which is apparently complex and is shown in Fig. 2a. Also shown is the TT fringe pattern (Fig. 2b) and the M slice result for Type A. It should be noted that fringe symmetry is not expected due to the difference in material fringe values for the two materials. The K_1 variation seems to be averaged out across the bond line. The TT value of 15.06 x 10^{-3} compares favorably with the L-M-R average of 14.65 x 10^{-3}. Although these results were
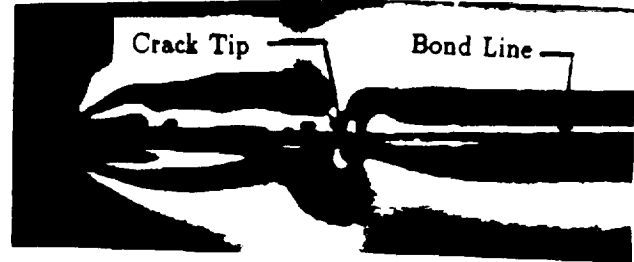
a) No Load (After Thermal Cycle)TT; MF = 2.65
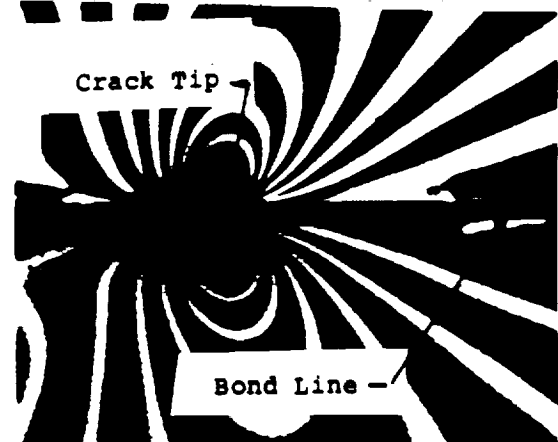
b) After Stress Freezing TT; MF = 10.10
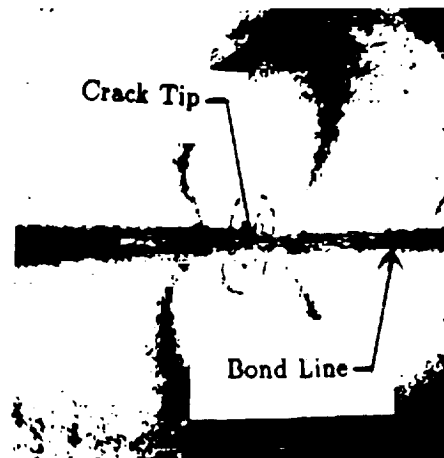
5th Multiple
c) Middle Slice; MF = 8.81

Fig. 2. Type A Fringe Patterns

not unreasonable, scatter in K_{AP} vs. $\sqrt{r/a}$ data and variations in bond thickness together with crack tip irregularities disturbed repeatability. Because of these problems, Type A specimens were replaced by Type B specimens.

Type B - Since bonding of the Type B specimen also resulted in a residual stress field it was decided to run two other tests in order to isolate the various effects. Test B-1 was a homogeneous araldite specimen with a Type B vee notch crack and Test B-2 was an araldite specimen with the same crack as B-1 but including a bondline.

The results of the Type B tests on all three Type B specimens are summarized in Table IV. The results presented in Table IV may be used to assess the Type B test specimen. The experimental results were corrected for the notch angle using the analysis of Gross and Mendelson [4].

Normally, for Mode I results data are taken across the crack plane from the top fringe loop to the bottom one and the result divided by two. This eliminates difficulties in locating the crack tip. This was not done in Table IV since loop data for Test B was not available for the Araldite - Aluminum specimen side. However, in this specimen, the crack tip location was obtained from a separate $40X$ photograph of the specimen surface which was overlaid on the fringe pattern for accuracy. In computing percentages, the Top and Bottom values were first averaged in B_1 and B_2 to eliminate error in locating the crack centerline, and then the L and R values were averaged to eliminate non-uniform loading effects through the thickness. Percent SIF variations through the thickness measured the difference between the central M value and the L and R values.

The fringe patterns from test B-1 were typical, showed no unusual results and are not shown here. Comparing the average of the slice results in B-1 with the theoretical K_1 value (Table IV) we see that the experimental results were 3.6% higher than the theoretical result, probably partially due to some machining residual stress. Fringe patterns in the B-2 specimens showed some residual stresses in the no load shot (Fig. 3a) resulting from curing of the bond line material, but loaded patterns appeared to swamp these stresses. By comparing the average of the slices with the theoretical results we see an increase at 8% over the theoretical value, of which 3.6% is assumed to be due to effects other than bond line curing.

The Type B fringe patterns are shown in Fig. 4. Fig. 4a shows a significantly higher near tip stress field due to the residual bond line stresses than for the B-2 specimen. Fig. 4b shows how the fringes are distorted

Table IV
K_1 Values from Specimens B-1, B-2 and B

L = Left side slice T = Above bond
M = Middle slice B = Below bond
R = Right side slice

$K_{Th} = 12.25 \times 10^{-3}$ MPa$\sqrt{m}$ Singular Zone $\sqrt{\frac{r}{a}}$ from .25 to 0.40

Specimen	$K_1 \times 10^3$ MPa$\sqrt{m}$
B1-L-T	13.24
B1-L-B	12.69
B1-M-T	12.60
B1-M-B	12.26
B1-R-T	13.05
B1-R-B	12.52

B2-L-T	
B2-L-B	13.34
B2-M-T	12.96
B2-M-B	13.00
B2-R-T	14.14
B2-R-B	13.16

B-L	14.24*
B-M	14.52
B-R	13.22*

* AVG 13.74

in the bondline. The middle slice is shown in Fig. 4c. By the same method of comparison as before, we see that the combined effects of machining, bond line and modulus increases K_1 by 14.2%.

Estimating the Effect of Residual Stress on K_1

The experimental methodology employed with the Type B test specimens allows one to assess the influence of the residual stresses on K_1 without a detailed analysis of the residual stress field produced by curing of the glue in the bond line. This is achieved by summarizing the results just discussed in Table V.
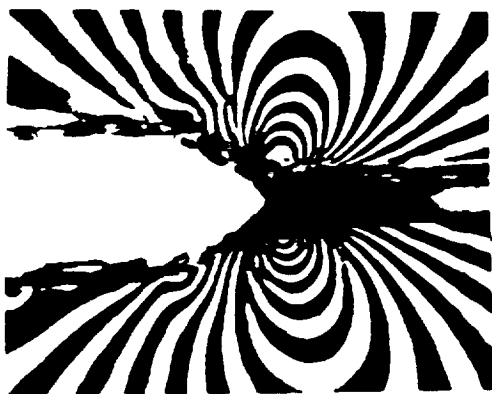
Table V

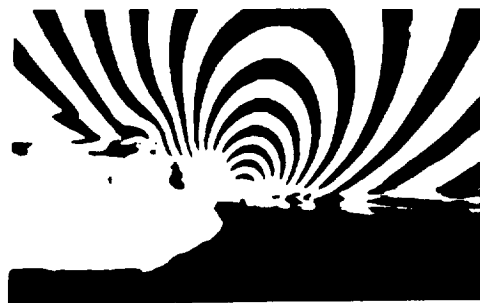| Specimen	Effect on K_1 (from slicing) of	Percent
B-1	Machining Stresses	+ 3.6
B-2	Machining Stress + Bond Line	+ 8.0
B	Machining Stress + Bond Line + Modulus	+ 14.2

a) No Load (After Thermal Cycle),

a) No Load (After Thermal Cycle),
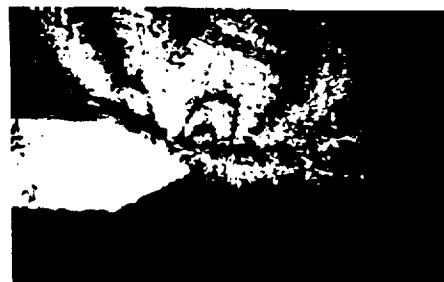

b) After Stress Freezing,

b) After Stress Freezing, MF = 8.70

5th Multiple
c) Side Slice,

Fig. 3 Type B-2 Fringe Patterns

5th Multiple
c) Middle Slice,

Fig. 4. Type B Fringe Pattern

(Bright Field) MF = 8.75

We conclude that the bond line effect in an otherwise homogeneous plate produces sufficient stress to increase K_1 4.4% when bonding dissimilar materials of modulus ratio of 2.13, the increase in K_1 due to the modulus effect is of the order of 6.20%. However this increase (6.20%) may be due to the no load thermal cycle (Fig. 3a and Fig. 4a).

Inclined Bond Line Cracks

When applied to bond line cracks which were tilted to the load direction, the type B specimens are currently under evaluation. It may turn out that a different crack thickness to bond thickness will be required in order to get accurate neartip reading. However, sufficient data have not yet been obtained to clarify this point. This study is in its early stages.

SUMMARY

A series of experiments involving two main types of cracked bimaterial specimens containing a bond line were conducted in order to assess the utility of the frozen stress method in measuring the variation of the SIF distribution through the specimen thickness and residual stress effects were assessed. It was found that:

(i) None of the loaded fringe patterns showed any evidence of a shear mode. It may be necessary to modify the Type B specimens for angled cracks.

(ii) Type A specimens were considered unsatisfactory.

(iii) Residual stresses were present in all tests. The effect of these stresses in the bi-material specimen can be separated from machining stresses as shown in Table V. Thus the increase in K_1 in B due to bond line curing and material mismatch was of the order of 10.6%. Thus the effect of the residual stress on K_1 can be assessed without measuring details of the residual stress.

(iv) Although a reasonable K_1 distribution through the thickness was obtained in B, indicating a measure of transverse constraint effect, the variation was judged to be of the order of the experimental scatter.

The present study is being expanded to include mixed mode loads and cracks parallel to the bond lines.

Note: The second page of the extended abstract of this paper (page 42 of the Extended Abstracts Proceedings) contained an error effecting the numerical results on that page. Those results have been corrected in the present paper.

References

[1] Rice, J.R., 1988, "Fracture Mechanics Concepts for Interfacial Cracks," *J. Ap. Mech.*, V. 55, pp. 98–103.

[2] Hutchinson, J.W. and Suo, A., 1992, "Mixed Mode Cracking in Layered Materials," *Advances in Applied Mechanics*, V. 29, Academic Press, pp. 63–191.

[3] Smith, C.W. and Kobayashi, A.S., 1993, "Experimental Fracture Mechanics," Ch. 20 of *Handbook on Experimental Mechanics*, 2nd Revised Ed., VCH Publishers, pp. 905–968.

[4] Gross, B. and Mendelson, A., 1972, "Plane Elastostatic Analysis of V-notched Plates," *Int. J. of Fracture Mechanics*, V. 8, N. 3, pp.267–276.

[5] Post, D. 1966, "Fringe Multiplication in Three Dimensional Photoelasticity," *J. of Strain Analysis*, V. 1n5, pp. 380-388.

[6] Tardy, M. L. H., 1929, "Methode Practique D'examen de Measure de la Birefringence des Verres D'optique," *Optics Rev.*, V. 8, pp. 59-69.
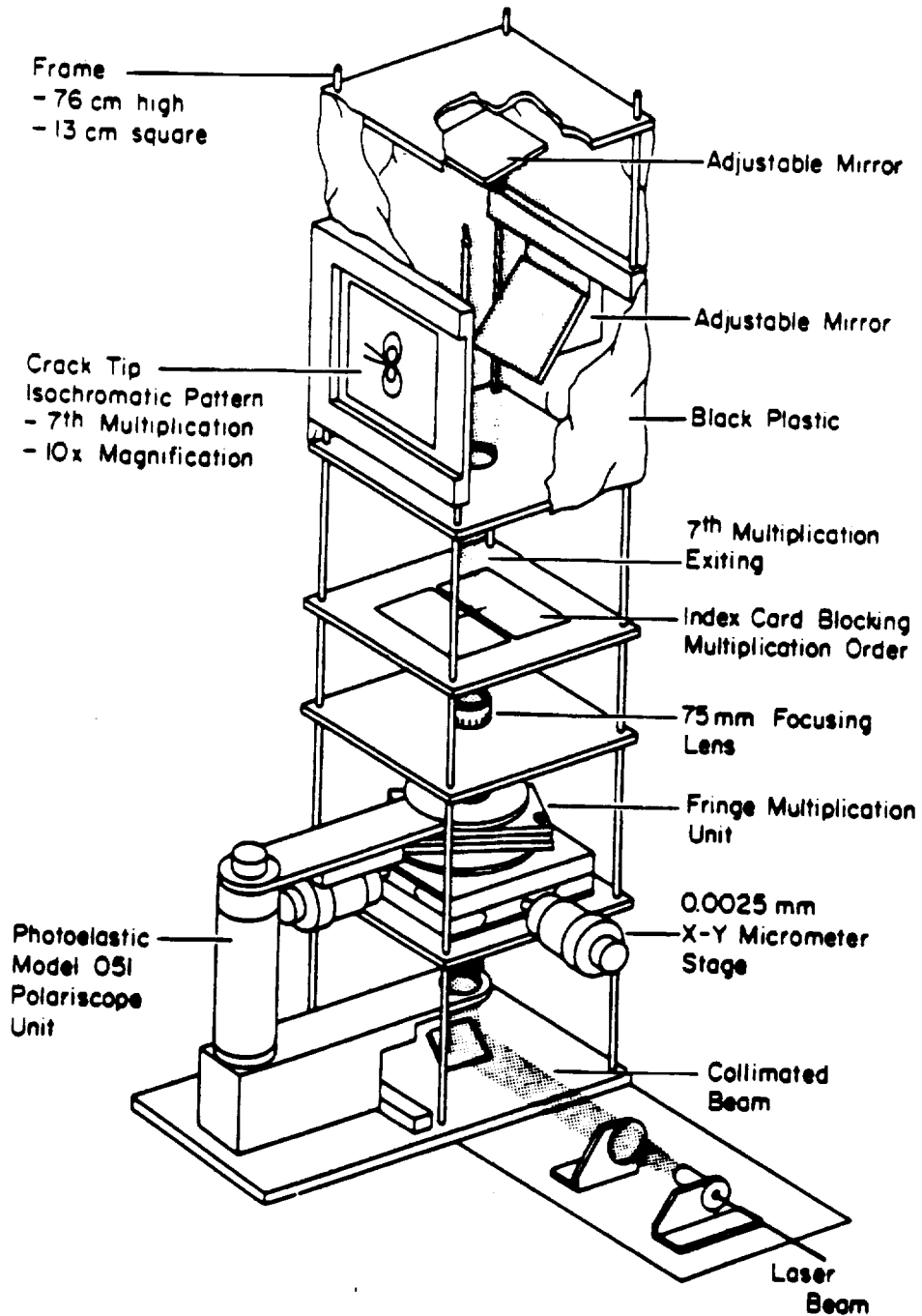
APPENDIX I - Frozen Stress Photoelasticity

When a transparent model is placed in a circularly polarized monochromatic light field, and loaded, dark fringes will appear which are proportional to the applied load. These fringes are called stress fringes or isochromatics and the magnitude of the maximum inplane shear stress is a constant along a given fringe.

Some transparent materials exhibit mechanical diphase characteristics above a certain temperature, called the critical temperature (T_c). The material, while still perfectly elastic will exhibit a fringe sensitivity of about twenty times the value obtained at room temperature and its modulus of elasticity will be reduced to about one six hundredth of its room temperature value. By raising the model temperature above T_c, loading, and then cooling slowly to room temperature, the stress fringes associated with T_c will be retained when the material is returned to room temperature. Since the material is so much more sensitive to fringe generation above T_c than at room temperature, recovery at room temperature upon unloading is negligible. The model may then be sliced without disturbing the "frozen in" fringe pattern and analyzed as a two dimensional model but containing the three dimensional effects. In the use of the method to make measurements near crack tips, due to the need to reduce loads above critical temperature to preclude

large local deformations, and the use of thin slices, few stress fringes are available by standard procedures. To overcome this obstacle, a refined polariscope (Fig. I-1) is employed to allow the tandem use of the Post (5) and Tardy (6) methods to increase the number of fringes available locally.

Frame
- 76 cm high
- 13 cm square

Adjustable Mirror

Adjustable Mirror

Crack Tip
Isochromatic Pattern
- 7th Multiplication
- 10x Magnification

Black Plastic

7th Multiplication
Exiting

Index Card Blocking
Multiplication Order

75mm Focusing
Lens

Fringe Multiplication
Unit

Photoelastic
Model 051
Polariscope
Unit

0.0025 mm
X-Y Micrometer
Stage

Collimated
Beam

Laser
Beam

II-2 Refined Transmission Polariscope

APPENDIX II

Mode I Algorithm for Homogeneous Case

Beginning with the Griffith-Irwin Equations, we may write, for Mode I,

$$\sigma_{ij} = \frac{K_1}{(2\pi r)^{\frac{1}{2}}} f_{ij}(\theta) + \sigma_{ij}^{\circ} \qquad (i.j. = n, z)$$

$$(II.1)$$

where:

σ_{ij} are components of stress

K_1 is SIF

r, θ are measured from crack tip (Fig. II-1)

σ_{ij}° are non-singular stress components.

Then, along $\theta = \pi/2$, after truncating σ_{ij}

$$(\tau_{nz})_{max} = \frac{K_1}{(8\pi r)^{\frac{1}{2}}} + \tau^{\circ} = \frac{K_{AP}}{(8\pi r)^{\frac{1}{2}}} \qquad (II.2)$$

where $\tau^{\circ} = f(\sigma_{ij}^{\circ})$ and is constant over the data range

K_{AP} = apparent SIF

τ_{nz} = maximum shear stress in nz plane

$$\therefore \frac{K_{AP}}{\bar{\sigma}(\pi a)^{\frac{1}{2}}} = \frac{K_1}{\bar{\sigma}(\pi a)^{\frac{1}{2}}} + \frac{\sqrt{8}\tau^{\circ}}{\bar{\sigma}} \left(\frac{r}{a}\right)^{\frac{1}{2}} \quad (II.3)$$

where (Fig. II.1) a = crack length, and $\bar{\sigma}$ = remote normal stress

i.e. $\dfrac{K_{AP}}{\bar{\sigma}(\pi a)^{\frac{1}{2}}}$ vs. $\sqrt{\dfrac{r}{a}}$ is linear.

Since from the Stress-Optic Law

$(\tau_{nt})_{max} = \frac{nf}{2t}$ where

n = stress fringe order

f = material fringe value

t = specimen (or slice) thickness

and from Eq. II.2

$K_{Ap} = (\tau_{nz})_{max}(8\pi r)^{\frac{1}{2}} = \frac{nf}{2t}(8\pi r)^{\frac{1}{2}}$,

then K_{Ap} (through a measure of n) and r became the measured quantities from the stress fringe pattern at different points in the pattern.

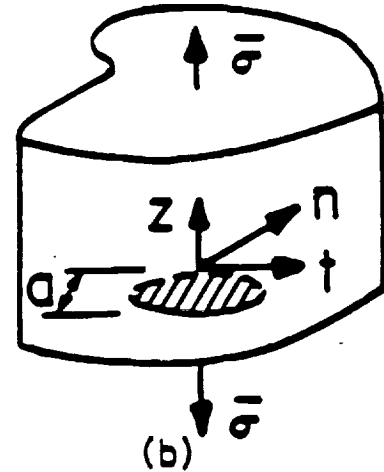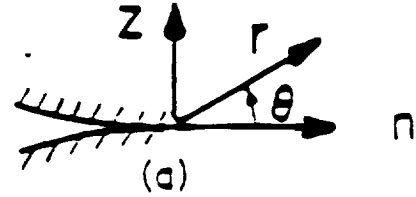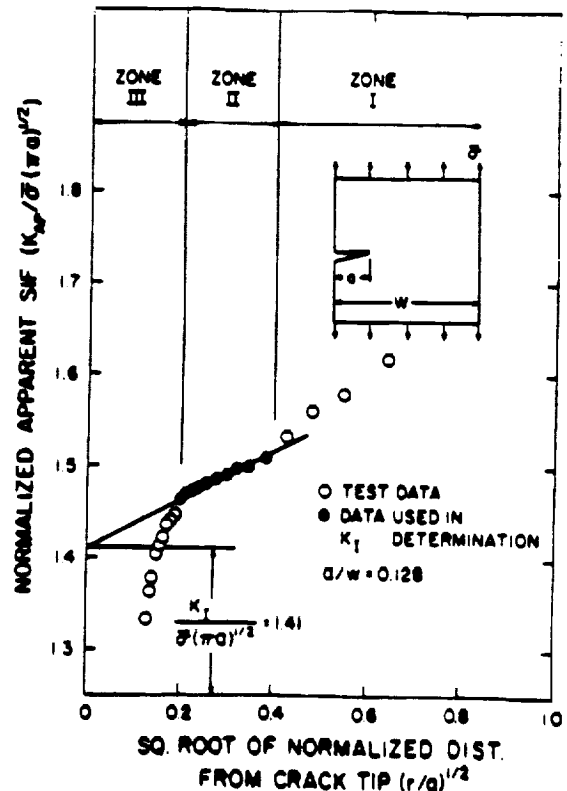A typical plot of normalized K_{AP} vs. $\sqrt{r/a}$ for a homogeneous specimen is shown in Fig. II.2.

Fig. II-1 Mode I Near Tip Notation

II-2 Determination of K_1 from Raw Test Data for a Homogeneous Specimen.

A METHOD FOR EVALUATING STRESS INTENSITY DISTRIBUTION FOR CRACKS IN ROCKET MOTOR BONDLINES

C. W. SMITH† and E. F. FINLAYSON

Department of Engineering Science and Mechanics. Virginia Polytechnic Institute and State University,
Blacksburg. VA 24061, U.S.A.

C. T. LIU

OL-AC PL RKS. Phillips Laboratory, 10 E. Saturn Boulevard. Edwards AFB, CA 93524-7680, U.S.A.

Abstract—A preliminary investigation limited to stress freezing materials was undertaken in order to develop a test method for estimating the stress intensity factor (SIF) distribution along the border of cracks in the bondline of a bimaterial specimen. It was desired to measure the influence of curing stress and mixed mode effects for such specimens. A single edge notched specimen was selected, and a test procedure was devised for isolating the curing stress effect at the bondline for Mode I. Subsequently, mixed mode tests were conducted and the SIF distributions for K_1 and K_2 were obtained. It was found that the level of the SIF values was increased by the bondline in cracked homogeneous bondline specimens for bondlines nearly normal to the applied load. but that this effect was not increased in bonded bimaterial specimens. For larger angles of inclination to a normal to the applied load. no increase in the SIF above the homogeneous result was found. © 1997 Elsevier Science Ltd

1. INTRODUCTION

WHEN A crack is located at the interface between two materials, near tip stress analysis is complicated by the fact that the mode 1 and mode 2 stress intensity factors (SIF) cannot be decoupled[1]. However, if the materials are incompressible, and plane strain exists, the near tip interface equations reduce to the more familiar form for isotropic and homogeneous elastic solids[2].

When cracks occur between a solid rocket motor and its rubber liner, the above conditions are approximately realized and occur at a rather low modulus ratio between the two materials. The first author and his colleagues have had considerable success in measuring three-dimensional effects in cracked isotropic and homogeneous bodies using a refined frozen stress method [3]. The frozen stress method is briefly summarized in Appendix A. In order to explore the feasibility of such an approach in measuring three-dimensional and curing stress effects in such cracks as described above, a series of experiments was conducted on thick plates in tension containing bondline cracks between two different incompressible materials.

2. SPECIMEN CONFIGURATION, MATERIALS AND TEST PROGRAM

The specimen configuration used in all tests is pictured in Fig. 1. All loads were parallel to the long dimension of the specimens. The materials and their properties are given in Table 1.

The thermal coefficient of expansion for both materials was matched exactly at 15.3×10^{-6} per °F at room temperature and $119 \times 10^{-6} \pm 20 \times 10^{-6}$ per °F at 240°F. The araldite–aluminum specimens were produced in opaque form by adding 25% by weight of aluminum powder to the pure transparent araldite, a common photoelastic material.

†Author to whom all correspondence should be addressed.

Units	a	W	l	t	h_b	h_c	d
m.m.	9.53	38.1	88.9	12.7	0.356	1.59	1.02
in.	0.375	1.50	3.50	0.500	0.014	0.063	0.040
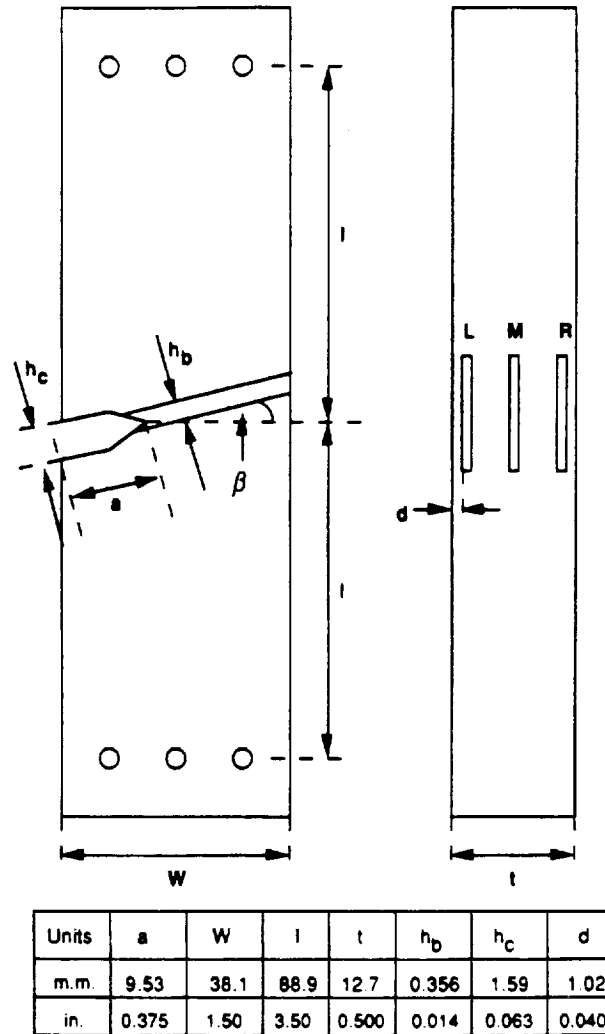
β = 0,15, 30 & 45 degrees

Fig. 1. Test geometry.

The bonding agent was a commercial glue PLM-9 made by Photolastic, Inc. Raleigh, N.C. The test specimen materials were supplied by Survey Technology Centre, London.

The testing program involved three test specimens for each crack orientation: one homogeneous specimen (B-1), one bonded homogeneous specimen (B-2) and one bonded bimaterial specimen (B). This was done in order to isolate residual bond line effects from bimaterial effects.

3. ANALYTICAL PROCEDURES

In order to provide an analytical control, the following procedure was used to estimate theoretical values of $K_{1(th)}$ and $K_{2(th)}$.

Table 1. Material properties

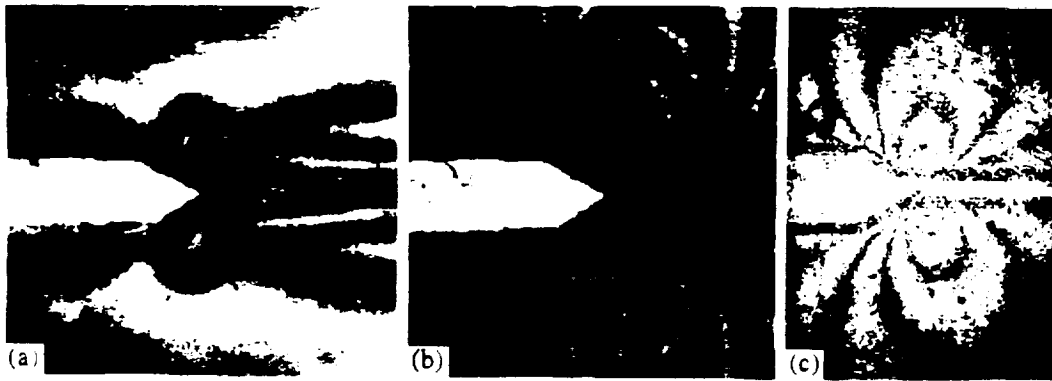| Material	$T_{critical}$	E_{Hot}	f_r
Araldite	240 F	2698 psi (18.60 MPa)	1.64 psi-in (286.9 Pa-m)
Aral-Alum	240 F	5349 psi (36.88 MPa)	—

Fig. 2. B-2 (homogeneous bonded specimen) for $\beta = 0°$. (a) No load (through thickness). (b) Loaded and stress frozen (through thickness). (c) Edge slice L (M.F. = 8.75).
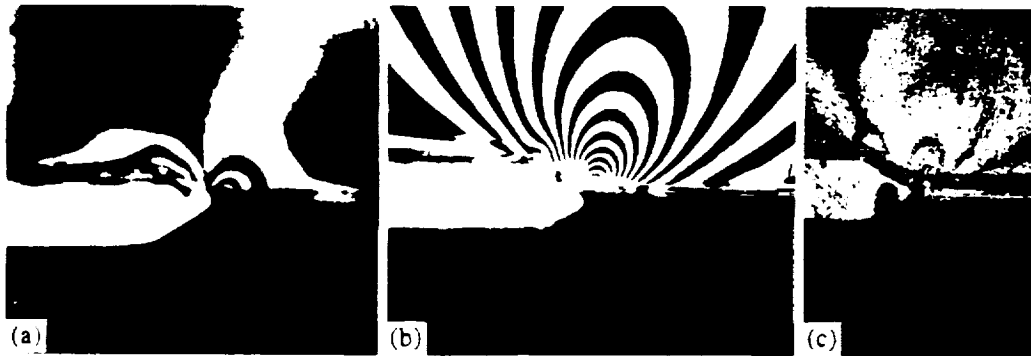

Fig. 3. B (bimaterial bonded specimen) for $\beta = 0°$. (a) No load (through thickness). (b) Loaded and stress frozen (through thickness). (c) Edge slice L (M.F. = 8.75).

The values of $K_{1(th)}$ and $K_{2(th)}$ were based on two-dimensional solutions for edge cracks in semi-infinite plates [4, 5], adjusted to finite width plates using refs [6, 7], and correcting for the notch effect using ref. [8]. In adjusting the infinite plate solution to the finite plate solution for inclined cracks ($\beta \neq 0$), the projection of the crack normal to the direction of the applied load was used.

Experimental results were obtained from frozen stress photoelastic experiments and optical data were converted into stress intensity values using the algorithms and procedures described in Appendix B.

4. TEST RESULTS

Frozen stress tests were conducted on edge cracked specimens for values of $\beta = 0°$, 15°, 30° and 45°. After stress freezing, thin slices were removed mutually orthogonal to the crack front and the crack plane (L,M,R in Fig. 1) and the slices were analyzed photoelastically (Appendix A) and SIF values were determined for each slice (Appendix B). Fringe patterns from the cracked homogeneous specimen were as expected and are not shown. Fringe patterns from the no load and loaded through thickness shots and an edge slice are shown for the homogeneous bonded specimen (B-2) in Fig. 2 for $\beta = 0°$. Corresponding photos for the bimaterial specimen for $\beta = 0°$ are shown in Fig. 3. Finally, corresponding photos for the homogeneous bonded specimen (B-2) are shown for $\beta = 30°$ in Fig. 4. It is clear that bond line curing fringes exist in all specimens but a developed singular fringe pattern does not exist for these cases. Machining stresses parallel to the notch sides appear to diminish during stress freezing.

In the 15° homogeneous bonded test, a crack emanated from the notch tip under load at the notch tip, ran to a bond-araldite interface and proceeded to grow along the interface.
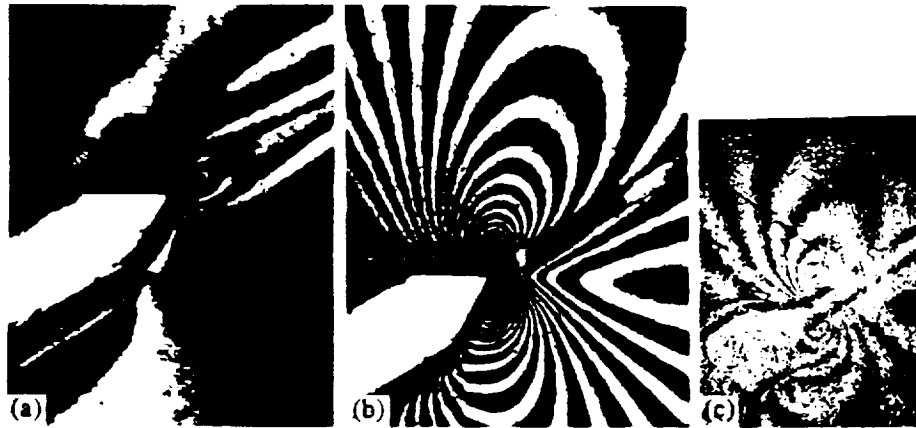
Fig 4. B-2 (homogeneous bonded specimen) for $\beta = 30^\circ$. (a) No load (through thickness). (b) Loaded and stress frozen (through thickness). (c) Edge slice L (M.F. = 8.75).

Table 2

Specimen	F_1	F_2	$F_1/(F_1)_{TH}$	$F_2/(F_2)_{TH}$
$\beta = 0^\circ$; [Fig. 1]; $(F_1)_{TH} = 1.51$ $\bar\sigma = 8.75$ psi (0.060 MPa)				
B1-LR	1.37	—	0.907	—
B1-M, LMR	1.67,1.47	—	1.11,0.974	—
B2-LR	1.73	—	1.15	—
B2-M, LMR	1.95,1.80	—	1.29,1.19	—
B-LR	1.72	—	1.14	—
B-M, LMR	1.82,1.75	—	1.21,1.16	—
$\beta = 15^\circ$; [Fig. 1]; $(F_1)_{TH} = 1.41$; $(F_2)_{TH} = 0.181$ $\bar\sigma_{B1} = 14.0$ psi (0.097 Mpa.); $\bar\sigma_{B2} = 8.75$ psi (0.060 Mpa.)				
B1-LR	1.31	0.179	0.929	0.989
B1-M, LMR	1.62,1.42	0.221,0.193	1.15,1.01	1.22,1.07
B-LR	1.52	0.209	1.08	1.15
B-M, LMR	1.79,1.61	0.244,0.231	1.27,1.14	1.35,1.28
$\beta = 30^\circ$; [Fig. 1]; $(F_1)_{TH} = 1.16$; $(F_2)_{TH} = 0.229$ $\bar\sigma_{B1} = 7.00$ psi (0.048 MPa); $\bar\sigma_{B2,B} = 14.0$ psi (0.097 MPa)				
B1-LR	1.03	0.3320	0.888	0.944
B1-M, LMR	1.14,1.07	0.353,0.330	0.983,0.922	1.04,0.973
B2-LR	1.05	0.323	0.905	0.953
B2-M, LMR	1.16,1.08	0.357,0.334	1.00,0.931	1.05,0.985
B-LR	1.02	0.317	0.879	0.935
B-M, LMR	1.16,1.07	0.357,0.330	1.00,0.922	1.05,0.973
$\beta = 45^\circ$; [Fig. 1]; $(F_1)_{TH} = 0.837$; $(F_2)_{TH} = 0.432$ $\bar\sigma = 7.00$ psi (0.048 MPa)				
B1-LR	0.856	0.494	1.02	1.14
B1-M, LMR	0.921, 0.877	0.532,0.506	1.10,1.05	1.23,1.17
B2-LR	0.843	0.486	1.01	1.13
B2-M, LMR	0.873, 0.852	0.504,0.492	1.04,1.02	1.17,1.14
B-LR	0.893	0.516	1.07	1.19
B-M, LMR	0.857, 0.881	0.494,0.508	1.02,1.05	1.14,1.18

$F_{TH} = $ 2D Theoretical estimates.
$F_1 = K_1/\bar\sigma\sqrt{\pi a}$; $F_2 = K_2/\bar\sigma\sqrt{\pi a}$
$a = 0.375$ in. (9.53 mm). [Fig 1]
B1 = Homogeneous specimen
B2 = Homogeneous bonded specimen
B = Bi-material specimen
LR = Average of left edge and right edge slices [Fig. 1]
LMR = Average of left edge, middle and right edge slices [Fig 1]
For $\beta \ne 0$, projections of mode 1 and mode 2 results are used.

The normalized SIF results from all tests are tabulated in Table 2. Several general comments can be made.

1. All F_{TH} values are two-dimensional analytical results. $(F_{II})_{TH}$ values are estimated from $(F_I)_{TH}$ analysis.
2. The F_I distributions through the thickness revealed a slight elevation in the SIF near midthickness as expected in every case except the 45°B-M result.
3. Only the 15° and 0° cases revealed a significant increase in $F_I/(F_I)_{TH_{AVG}}$ in the bimaterial specimens (14%, 16%). However, this same order of increase was found for the 0° homogeneous bonded specimen (19%) and would be expected for the 15° case as well.
4. Values of $\{F_{II}/(F_{II})_{TH}\}_{AVG}$ were generally higher than their $\{F_I/(F_I)_{TH}\}_{AVG}$ counterparts but, since we do not have an accurate two-dimensional analytical result for this case, no particular significance is attached to these elevations.

5. SUMMARY

A series of tests was conducted in order to provide a data base for the development of a test for evaluating stress intensity factor distributions along bond lines between incompressible materials of different Moduli of Elasticity. It was desired to separate the bond line effect from the bimaterial effect (see Table 3).

As shown in Table 2, variations in the SIF across the plate thickness were small and of the order of the accuracy of the method of analysis (2.6%). However, they did show the expected distribution in the bimaterial specimen. Moreover, the procedure allows separation of bond stress and bimaterial stress effects.

Tests were conducted on specimens containing bondline artificial cracks inclined to the load direction at the angles of 0°, 15°, 30° and 45°. The modulus ratio in the bimaterial specimens was 1.97. Stress intensity factors determined at intervals through each specimen thickness by the frozen stress method were normalized with respect to two-dimensional solutions for Mode I and two-dimensional estimates for Mode II.

As a result of these studies, it was found that:

1. For $\beta = 0°$ and $\beta = 15°$, a significant elevation in K_I occurred in the bimaterial specimens (14% to 16%). However, this increase also occurred in the homogeneous bonded specimen in the $\beta = 0°$ test and is expected in the $\beta = 15°$ homogeneous bonded test. The suggestion is that the elevation of K_I is due to the bondline stresses and not due to the modulus ratio in the bimaterial specimen. Examination of the no load bondline fringes reveals that they are indeed nearly normal to the load direction near the crack tip.
2. It is of interest to note that there was no effect on K_I of either the homogeneous bondline or the bimaterial specimen for values of $\beta = 30°$ and 45°. This is believed due to the fact that the no load bondline fringes were nearly parallel to the load direction near the crack tip and thus made no contribution to the fringe gradient in the load direction which is used to determine K_I. A qualitative sketch of the effect of the bondline residual stress in (1) and (2) is shown in Fig. 5.
3. Mode II results were larger than predicted by approximate analysis, but again appeared due solely to bondline effects.
4. In all cases except one the peak SIF occurred at mid-thickness. In the single exception, ($\beta = 45°$) the variation in the SIF across the thickness appeared to be of the order of the experimental scatter (i.e. $< \pm 3\%$).

Table 3 Thickness averaged results compared to the 2D homogeneous solution for $\beta = 0°$

Specimen	Effect on K_I of	Percent
B-1	Machining stresses	−2.60
B-2	Machining stress + bondline stress	19
B	Machining stress + bondline + modulus	16

EFM 9/1-2 D

For β = 0°, 15°
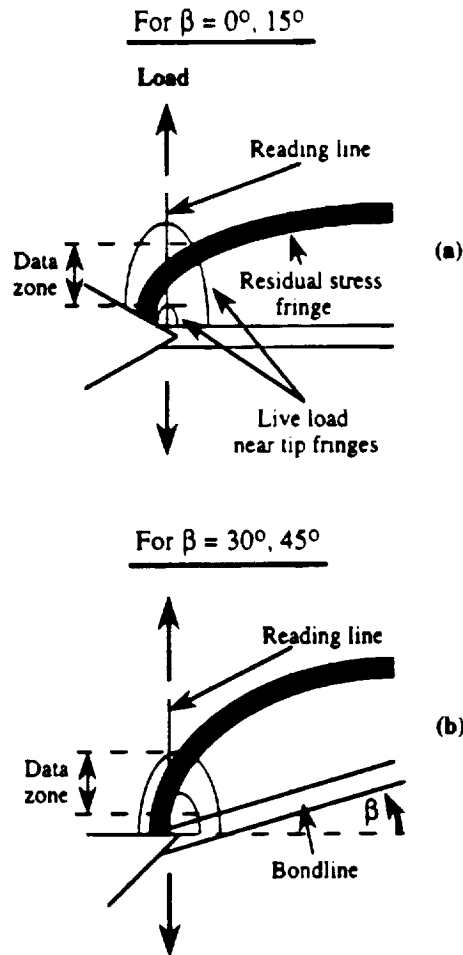

(a)

For β = 30°, 45°

(b)

Fig. 5. Artist's rendition of bond line stress effect.

In conclusion, it appears that using the three specimen test procedure, reasonable results can be obtained for SIF distributions through the thickness of bimaterial specimens containing bondline cracks in incompressible materials. Tests employing this method are being conducted on cracks parallel to the bond line.

REFERENCES

1 Rice. J. R.. Fracture mechanics concepts for interfacial cracks. *J. appl. Mech.*, 1988, **55**, 98–103.
2 Hutchinson. J. W. and Suo. A.. Mixed mode cracking in layered materials. *Advances in Applied Mechanics*, 1992, **29**, 63–91.
3 Smith. C. W. and Kobayashi. A. S.. Experimental fracture mechanics. In *Handbook on Experimental Mechanics*. 2nd edn. Chap. 20. VCH Publishers. 1993. pp. 905–968.
4 Hasebe. N. and Inohara. S.. Stress analysis of a semi-infinite plate with an oblique edge crack. *Ing. Arch.*, 1980. 49, 51–62.
5 Isida. M.. Tension of a half plane containing array cracks. branched cracks and cracks emanating from sharp notches. *Trans. Japan Soc. of Mechanical Engineers*, 1979. 45(392), 306–317.
6 Gross. B., Srawley. J. E. and Brown. W. F., Jr. Stress intensity factors for a single edge notched tension specimen by boundary collocation of a stress function. Report NASA. Lewis. 1964.
7 Bowie. O. L., Rectangular tensile sheet with symmetric edge cracks. *J. appl. Mech.*, 1964. 31(2), 208–212.
8 Gross. B. and Mendelson. A.. Plane elastostatic analysis of V-notched plates. *Int. J. Fracture Mech.*, 1972. 8(3). 267–276.
9 Post. D.. Fringe multiplication in three dimensional photoelasticity. *Journal of Strain Analysis*, 1966. 1(5), 380–388.
10 Tardy. M. L. N.. Methode practique examen de measure de la birefringence des verres d'optique. *Opt. Rev.*, 1929. 18, 59–69.

APPENDIX A

Frozen stress photoelasticity

When a transparent model is placed in a circularly polarized monochromatic light field, and loaded, dark fringes will appear which are proportional to the applied load. These fringes are called stress fringes or isochromatics and the magnitude of the maximum in-plane shear stress is a constant along a given fringe.

Some transparent materials exhibit mechanical diphase characteristics above a certain temperature, called the critical temperature (T_c). The material, while still perfectly elastic will exhibit a fringe sensitivity of about 20 times the value obtained at room temperature and its modulus of elasticity will be reduced to about one six hundredth of its room temperature value. By raising the model temperature above T_c loading, and then cooling slowly to room temperature, the stress fringes associated with T_c will be retained when the material is returned to room temperature. Since the material is so much more sensitive to fringe generation above T_c than at room temperature, fringe recovery at room temperature upon unloading is negligible. The model may then be sliced without disturbing the "frozen in" fringe pattern and analyzed as a two-dimensional model, but containing the three-dimensional effects. In the use of the method to make measurements near crack tips, due to the need to reduce loads above critical temperature to preclude large local deformations, and the use of thin slices, few stress fringes are available by standard procedures. To overcome this obstacle, a refined polariscope is employed to allow the tandem use of the Post[9] and Tardy[10] methods to increase the number of fringes available locally.

In fringe photographs, integral fringes are dark in a dark field and bright in a bright field. Bright fields are used throughout this paper for clarity.

APPENDIX B

Mode I algorithm for homogeneous case

Beginning with the Griffith-Irwin Equations, we may write, for Mode I,

$$\sigma_{ij} = \frac{K_1}{(2\pi r)^{1/2}} f_{ij}(\theta) + \sigma_{ij}^c \quad (i,j = n,z). \tag{B1}$$

where σ_{ij} are components of stress, K_1 is SIF, r, θ are measured from the crack tip (Fig. 6), σ_{ij} are non-singular stress components.

Then, along $\theta = \pi/2$, after truncating σ_{ij}

$$(\tau_{nz})_{max} = \frac{K_1}{(8\pi r)^{1/2}} + \tau^\circ = \frac{K_{AP}}{(8\pi r)^{1/2}}. \tag{B2}$$

where $\tau^\circ = f(\sigma_{ij}^c)$ and is constant over the data range, $K_{AP} =$ apparent SIF, $\tau_{nz} =$ maximum shear stress in nz plane.

$$\therefore \quad \frac{K_{AP}}{\bar{\sigma}(\pi a)^{1/2}} = \frac{K_1}{\bar{\sigma}(\pi a)^{1/2}} + \frac{\sqrt{8}\tau^\circ}{\bar{\sigma}} \left(\frac{r}{a}\right)^{1/2}. \tag{B3}$$

where (Fig. 6) $a =$ crack length and $\bar{\sigma} =$ remote normal stress, i.e. $K_{AP}/\{\bar{\sigma}(\pi a)^{1/2}\}$ vs $\sqrt{r/a}$ is linear.

Since from the Stress-Optic Law, $(\tau_{nz})_{max} = \frac{nf}{2t}$, where $n =$ stress fringe order, $f =$ material fringe value, $t =$ specimen (or slice) thickness and from eq. (B2), then
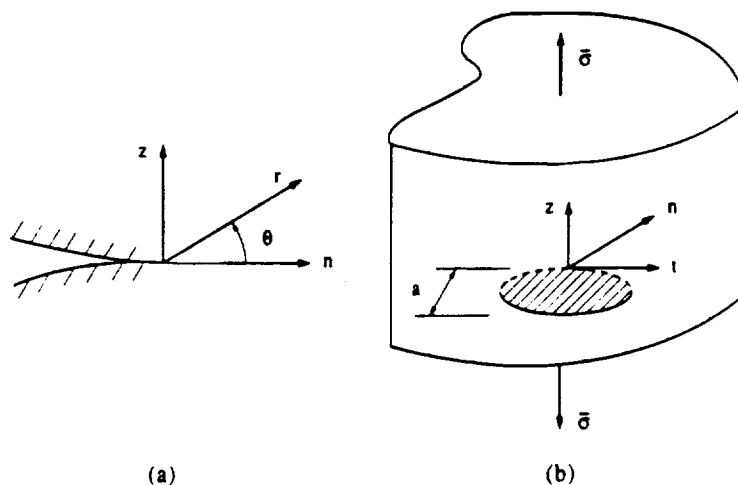

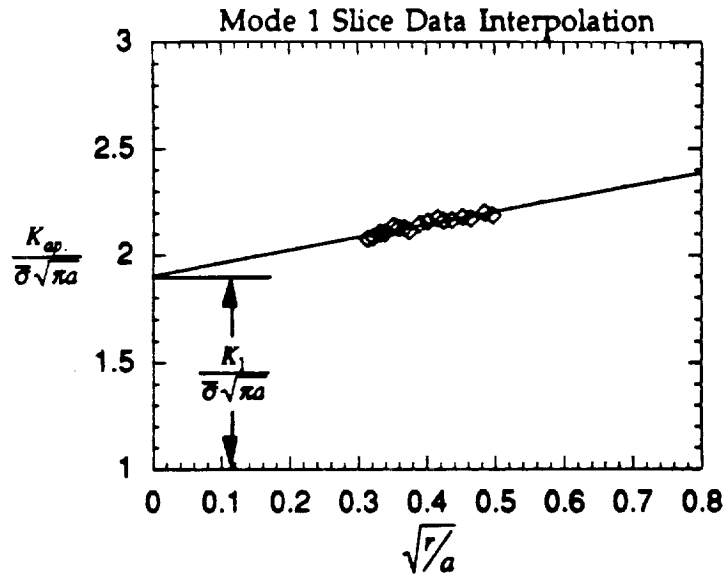
(a)   (b)

Fig. 6. Near tip notation.

Mode 1 Slice Data Interpolation

Fig. 7. Determination of $K_1/\bar{\sigma}\sqrt{r/a}$ from test data

$$K_{AP} = (\tau_{n.z})_{max}(8\pi r)^{1/2} = \frac{nf}{2t}\,(8\pi r)^{1/2},$$

and K_{AP} (through a measure of n) and r become the measured quantities from the stress fringe pattern at different points in the pattern.

A typical plot of normalized K_{AP} vs $\sqrt{r/a}$ for a homogeneous specimen is shown in Fig. 7.

Mixed mode algorithm

The mixed mode algorithm was developed (see Fig. 8) by requiring that:

$$\lim_{\substack{r_m \to 0 \\ \Theta_m \to \Theta_m^c}} \left\{ (8\pi r_m)^{1/2}\frac{(\partial\tau)_{n.z}^{max}}{\partial\Theta}(K_1, K_2, r_m, \Theta_m, \tau_{ij}) \right\} = 0. \tag{B4}$$
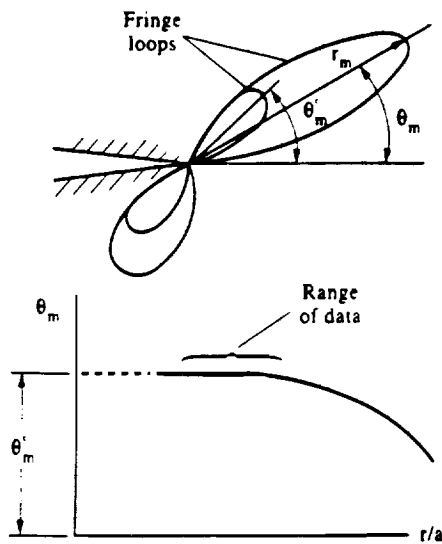
which leads to:

Fig. 8. Determination of θ_m^c for mixed mode case.

$$\left(\frac{K_2}{K_1}\right)^2 - \frac{4}{3}\left(\frac{K_2}{K_1}\right)\cot 2\Theta_m - \frac{1}{3} = 0. \tag{B5}$$

By measuring Θ_m which is approximately in the direction of the applied load, K_2/K_1 can be determined. Then writing

$$\tau_{n_z}^{max} = \frac{fn}{2t} = \frac{K_{AP}^*}{(8\pi r)^{1/2}}.$$

one may plot $K_{AP}^*/(\sigma(\pi a)^{1/2})$ vs $\sqrt{r/a}$ as before, locate a linear zone and extrapolate to $r = 0$ to obtain K^*. Knowing K^*, K_2, K_1 and Θ_m values of K_1 and K_2 may be determined since

$$K^* = [(K_1 \sin \Theta_m^2 + 2K_2 \cos \Theta_m^2)^2 + (K_2 \sin \Theta_m^2)^2]^{1/2}. \tag{B6}$$

Details are found in ref. [3]. A plot of $K_{AP}^*/\bar{\sigma}\sqrt{\pi a}$ vs $\sqrt{r/a}$ will yield a linear zone from which K^* can be extracted. Knowing K^* and Θ_m, K_1 and K_2 can be determined from eqs (B5) and (B6).

BOND LINE RESIDUAL STRESS EFFECTS ON CRACKS PARALLEL TO THE BOND LINES IN RUBBERLIKE MATERIALS

C. W. Smith and E.F. Finlayson

Department of Engineering Science and Mechanics
Virginia Polytechnic Institute and State University
Blacksburg, VA 24061

C. T.Liu
Phillips Laboratory
Edwards AFB, CA

ABSTRACT

Using the frozen stress photoelastic method, stress intensity factor (SIF) distributions through the thickness of plates containing blunt through cracks parallel to and at different distances from the bond line between materials of the same and different moduli are determined. By comparing the homogeneous bonded with the bi-material specimens while suppressing the influence of differing critical temperatures, the effect of modulus mismatch is estimated as well as bond line effects.

1. INTRODUCTION

Solid rocket motors consist of an incompressible matrix which lends itself to being modelled by frozen stress photoelasticity above the critical temperature (T_c) of the material. The first author and his colleagues have analyzed SIF distributions along crack fronts in rocket motor models (Smith and Wang, 1992) and (Smith et al, 1993) and recently have measured SIF distributions along crack fronts in bond lines between two materials of the same and different moduli using a refined frozen stress method (Smith et al, 1997). In the latter paper, since the material was incompressible above T_c and the test specimens were relatively thick, the interface fracture equations (Hutchinson and Suo, 1992) reduced to the classical, homogeneous form for near tip nearly plane

strain states.

When cracks in rocket motor material are loaded in a moderate temperature regime, significant blunting results at the crack tip. Moreover, such cracks occasionally form parallel to the bond line. The present study was undertaken in order to establish the extent of the influence of bond line stresses upon the SIF distribution along the blunted crack fronts for cracks parallel to bond lines in both homogeneous bonded and bi-material specimens.

2. TEST SPECIMENS AND METHOD OF ANALYSIS

Edge cracked specimens, the dimensions of which are presented in Fig. 1, were selected for the analysis. Three types of specimens were used:

a) One without a bond (used as a control).

b) Bonded homogeneous specimens to measure the effect of the bond stresses.

c) Bi-material specimens to assess the combined influence of modulus and T_c mismatch in the two materials while suppressing effects due to T_c mismatch as much as possible.

Specimens of each type were first cycled through a stress freezing cycle under no live load, then loaded, stress frozen. and three slices (L,M,R in Fig. 1) were removed from each specimen and analyzed using a refined frozen stress procedure. The frozen stress concept is described in Appendix I and algorithms for converting photoelastic data into SIF values at points along the crack border are described in Appendix II.

According to interface fracture mechanics theory (Hutchinson and Suo, 1992), under conditions of material incompressibility and plane strain for a bond line crack, there will be no modulus mismatch effect upon the SIF. This result was confirmed in some prior tests (Smith et al, 1997) using araldite bonded to araldite containing aluminum powder. The two materials exhibited the same T_c but their thermal coefficients were somewhat different above T_c.

In producing stress freezing materials, manufacturers have apparently had to sacrifice control of T_c in order to maintain accurate values of material fringe value, thermal coefficient variations, hot modulus and general material quality. Consequently, in the present study, two commercial materials with the same thermal coefficients but different T_c values were selected and tested in order to assess the effect of the T_c - modulus mismatch.

Cracks were machined into the material with the higher T_c in order to minimize the influence of T_c mismatch, since the material with lower T_c would still be in the rubbery state when the material with the higher T_c becomes glassy and so should have a smaller influence on crack tip residual stress than if the crack were in the material with the lower T_c.

The two materials used were PLM-4B and PSM-9 with properties as given in Table I.

Table I - Material Properties

Material	$T_{critical}$	E_{Hot}	f
PLM-4B	180°F	(12.96 MPa)	(420.3 Pa-m)
PSM-9	205°F	(47.67 MPa)	(520.1 Pa-m)

These materials were produced by Photoelastic Inc. and specified to have the same thermal coefficients at room temperature (T_R) and critical temperature (T_c). They were given as $\alpha_{RT} = 39 \times 10^{-6}/°F$ and $\alpha_{CT} = 90 \times 10^{-6}/°F$ respectively.

PLM-4B was used in the control and homogeneous bond line specimens and cracks were located at three different distances from the bond line. In the bimaterial specimens, the crack was located in the PSM-9. The bond line glue was chemically the same as PSM-9 but was used in liquid form when applied. The test procedure followed was the following:

i) Prepare test specimen blanks with loading holes and check in a polariscope for any fringes. If present. discard blanks.

ii) Insert cracks in specimen blanks using a Buehler diamond saw.

iii) Glue specimen blanks together to form test specimens and run a no load stress freezing thermal cycle to complete curing of bond line glue and assess T_c mismatch effect.

iv) Stress freeze specimens.

v) Remove three thin slices mutually orthogonal to crack plane and its border from each specimen.

vi) Analyze slices in refined polariscope and convert optical data into SIF values for each slice using the algorithms in Appendix II.

The blunted crack pushed the singular data zone further from the crack tip than for a sharp crack and produced somewhat elevated SIF values in the homogeneous specimen. However this is not expected to affect the normalized comparisons made in the present test program.

3. RESULTS

A. Homogeneous Bonded Specimens

After bonding, a single stress freezing cycle with no applied load was carried out. Fig. 2 shows the through thickness (TT) stress fringe field developed in the curing cycle for B-1($h = 12.7$ mm) and indicates no interaction between the crack and the bond line stress. Moreover, the data zone normal to and passing through the crack tip is completely free of fringes indicating no effect on the K_1 or non-singular values due to T_c mismatch. For B-2 ($h = 6.35$ mm) interaction was observed and for B-3 ($h = 3.17$ mm) a significant interaction between crack and bond line resulted. However, all of the data zone used for computing K_1 and K_2 except B-5 are completely within the same fringe order. This indicates a change in σ_{ij}^0 but not in K_1 or K_2. The effect on B-5 is noted in the next section. In all cases, one fringe was clearly visible adjacent to the bond line.

Both the control specimen B and the B-1 ($h = 12.7$ mm) specimens yielded pure Mode I fringe patterns which were the same to within ±5%, a range established by determining K_1 on each side of the control specimen. Consequently their fringe patterns revealed no new information and are not shown. Fringe patterns for B-2 ($h = 6.35$ mm) still showed a pure Mode I field but K_1 was slightly reduced by the curing stress field. Fig. 3 shows a TT and a slice fringe pattern for B-3 ($h = 3.17$ mm) and indicates a disturbance in the near

tip field on the side nearest the bond line.

There was no evidence of a shear mode near the tip in any of the fringe patterns which were read to within 0.02 of a stress fringe. Using the Mode I algorithm described in Appendix II the normalized apparent SIF was plotted vs. $\sqrt{r/a}$, over a linear zone between $\sqrt{r/a}$ of 0.35 to 0.6, the slope of which is proportional to the non-singular stress field was found. A typical plot is shown in Fig. II-2 for data on the side of the crack above it.

For the B-3 specimen, this plot for data below the crack revealed that the nonsingular field was significantly altered between the crack and the bond line and the slope was reversed. This is interpreted to mean that the treatment in the algorithm of a constant non-singular stress field was not valid within the measurement zone below the crack. Consequently all K determinations were made on fringes on the side of the crack away from the bond line. Results from slice data are given in Table II and show significant K_1 elevation near mid thickness.

Table II
Bonded Homogeneous Specimen Results

Specimen	F_1	F_1/F_{CTT}
B-1(LR)	1.53	0.93
B-2(LR)	1.47	0.90
B-3(LR)	1.65	1.01
B-1(M)	1.93	1.18
B-2(M)	1.81	1.10
B-3(M)	1.85	1.13
B-1(LMR)	1.66	1.01
B-2(LMR)	1.58	0.97
B-3(LMR)	1.72	1.05

TT = Through Thickness

LR = Average value of left and right side slices

M = Middle slice value

LMR = Average value of left side, middle, and right side slices

K_1 = mode 1 stress intensity factor

σ = Nominal far field stress

a = crack length

$F_1 = K_1/\sigma(\pi a)^{1/2}$

F_{CTT} = Normalized mode 1 stress intensity factor corresponding to LMR slice average of homogeneous control specimen

B. Bi-material Specimens

For the bi-material specimens, B-4, B-5 and B-6, after the curing cycle, interaction was found between the bond line stress and the crack tip for all three cracks. As shown in Fig. 4, the bond line fringe for B-4 is broader than in the homogeneous case but the stress level was similar. When the bi-material specimens were loaded and stress frozen, contraction of the PSM-9 as it passed through its critical temperature ($205°F$) during cooling was slightly restrained by the PLM-4B which was still above its $T_c(180°F)$ (i.e. $E_{rubbery}/E_{glassy} < 0.5\%$). When the PLM-4B changed into it's glassy state, the corresponding shrinkage would impose a small live stress field in the PSM-9. However, when slices were removed to take data, this stress would be likely released. Loading added a shear mode to specimens B-4, B-5 and B-6 as shown in Fig. 5.

The inclination of the reading line angle near the crack tip increased as h decreased. Thin slices were removed from each specimen and analyzed as before using the mixed mode algorithm of Appendix II. The results of this analysis are shown in Table III.

Table III
Bimaterial Specimen Results

Specimen	F_1	F_2	F_1/F_{CTT}	F_2/F_{CTT}
B-4(LR)	1.53	0.11	0.93	0.07
B-5(LR)	1.70	0.20	1.04	0.12
B-6(LR)	2.01	0.31	1.23	0.19
B-4(M)	1.96	0.14	1.20	0.09
B-5(M)	1.81	0.21	1.10	0.13
B-6(M)	2.35	0.37	1.43	0.23
B-4(LMR)	1.67	0.12	1.02	0.07
B-5(LMR)	1.74	0.20	1.06	0.12
B-6(LMR)	2.12	0.33	1.29	0.20

TT = Through Thickness

LR = Average value of left and right side slices

M = Middle slice value

LMR = Average value of left side, middle, and right side slices

K_1 = mode 1 stress intensity factor

σ = Nominal far field stress

a = crack length

$F_1 = K_1/\sigma(\pi a)^{1/2}$

$F_2 = K_2/\sigma(\pi a)^{1/2}$

F_{CTT} = Normalized mode 1 stress intensity factor corresponding to LMR slice average of homogeneous control specimen

4. DISCUSSION OF RESULTS

From the fringe patterns obtained for the homogeneous bonded specimens, it is clear that only Mode I exists near the crack tip although shear was present globally. From Table II the ratios of the normalized SIF in the middle slices to those near the edges were $1.93/1.53 = 1.26$ for B-1; $1.81/1.47 = 1.23$ for B-2, and $1.85/1.65 = 1.12$ for B-3. Since the accuracy of the method is judged to be $\pm 5\%$, these "thumbnailed" distributions are readily measured. The presence of the bond line does not influence the B-1 crack. (i.e. $F_1/F_{CTT} = 1.01$) Variations in B-2 and B-3, causing an SIF reduction in B-2 but an increase in B-3 are likely not significant.

The results from the analysis of the test data from the bi-material tests are presented in Table III. The results clearly show the presence of a shear mode. There is also a significant increase in the SIF near the mid-thickness of both F_1 and F_2. Comparing average values from Tables II and III, it is clear that the effect on F_1 is negligible for B-4, small for B-5 but becomes significant for B-6, with the bi-material values of LMR exceeding those of the homogeneous bonded values near the bond line. It is again clear that the distribution in the SIF through the thickness is measurable in the bi-material specimens. For example, the ratios:

B-4M/B-4LR $= 1.96/1.53 = 1.28$

B-5M/B-5LR $= 1.81/1.70 = 1.06$

B-6M/B-6LR $= 2.35/2.01 = 1.17$

are all easily measured differences across the thickness. Moreover, the no-load photo for B-5 revealed a full fringe around the crack tip which is estimated to increase the B-5 K results by as much as 8%. The above results suggest that this no load fringe may only have affected the edge slices LR.

Finally, one may conjecture that, from the point of view of a designer, when the crack is located further from the bond line than its own length, the effect on the Mode I SIF is negligible and the shear mode effect is of the order of 7% of the Mode I control value. For a crack only one third its length from the bond line the Mode I SIF is increased by about 29% above control while the Mode II effect is about 20% of the control value.

In (Smith et al, 1997), when a crack was placed in the bond line between two materials of the same T_c but different moduli, the average SIF was the same as for a companion cracked homogeneous bonded specimen, suggesting that the modulus mismatch has no influence on the SIF. Assuming that to be the case, we might then attribute the presence of Mode II and the increase in Mode I in B-6 entirely to the T_c mismatch. On the other hand, since we have tried to minimize T_c effects and none can be detected when comparing TT no load curing cycle fringe patterns of B-1, B-2, and B-3 with B-4, B-5 and B-6, (except possibly the SIF distribution in B-5 as noted earlier) one is inclined to conjecture that the increase in the Mode I SIF in B-6 might be due primarily to the modulus mismatch. However, pending further studies this result must remain an open question.

These studies reveal the importance of exercising careful control over the T_c, cure, and thermal coefficient control when using bi-material specimens for stress freezing. On the other hand, accurate variations in the SIF values through the thickness can be measured.

REFERENCES

Hutchinson, J.W. and Suo, H., 1992, "Mixed Mode Cracking in Layered Materials" *Advances in Applied Mechanics* V29 Academic Press, pp. 63-91.

Post, D., 1966, "Fringe Multiplication in Three Dimensional Photoelasticity" *Journal of Strain Analysis* V1 n5, pp 380-388.

Smith, C.W. and Wang., L., 1992, "Stress Intensity Factor Distribution and Crack Shapes in 3D Problems Using Frozen Stress" *Advances in Local Fracture/Damage Models for the Analysis of Engineering Problems* J.H. Giovanola and A.J. Rosakis Eds. ASME AMD Vol. 137 p. 109-120.

Smith, C.W. Wang L., and Liu, C.T., 1993, "Experimental Determination of Crack Growth and SIF Determination in Motor Grain Models" *Novel Experimental Techniques in Fracture Mechanics* A. Shukla, Ed. ASME AMD Vol. 176 p. 101-112.

Smith, C.W., Finlayson, E.F., and Liu, C.T., 1997, "Studies of Artificial Cracks at Rocket Motor Liners by the Frozen Stress Method" *Proc. of 1996 JANNAF Propulsion and Joint Subcommittee Meetings* C.P.I.A. Publ. #652 p. 201-212.

Smith, C.W. and Kobayashi, A.S. 1993, "Experimental Fracture Mechanics" *Ch 20 of Handbook on Experimental*

Mechanics 2nd Ed. A.S. Kobayashi, Ed. VCH Publishers, pp. 905-968.

Tardy, M.L.H., 1929, "Methode Practique D'examen deMeasure de la Birefringence des Verres D'optique *Optics Review* V8, pp. 59-69.

APPENDIX I - Frozen Stress Photoelasticity

When a transparent model is placed in a circularly polarized monochromatic light field, and loaded, dark fringes will appear which are proportional to the applied load. These fringes are called stress fringes or isochromatics and the magnitude of the maximum inplane shear stress is a constant along a given fringe.

Some transparent materials exhibit mechanical diphase characteristics above a certain temperature, called the critical temperature (T_c). The material, while still perfectly elastic will exhibit a fringe sensitivity of about twenty times the value obtained at room temperature and its modulus of elasticity will be reduced to about one six hundredth of its room temperature value. By raising the model temperature above T_c, loading, and then cooling slowly to room temperature, the stress fringes associated with T_c will be retained when the material is returned to room temperature. Since the material is so much more sensitive to fringe generation above T_c than at room temperature, fringe recovery at room temperature upon unloading is negligible. The model may then be sliced without disturbing the "frozen in" fringe pattern and analyzed as a two dimensional model but containing the three dimensional effects. In the use of the method to make measurements near crack tips, due to the need to reduce loads above critical temperature to preclude large local deformations, and the use of thin slices, few stress fringes are available by standard procedures. To overcome this obstacle, a refined polariscope (Fig. I-1) is employed to allow the tandem use of the Post (Post, 1966) and (Tardy, 1929) methods to increase the number of fringes available locally.

In fringe photographs, integral fringes are dark in a dark field and bright in a bright field. Dark fields are used throughout this paper.

APPENDIX II (Algorithms)

Mode I Algorithm for Homogeneous Case

Beginning with the Griffith-Irwin Equations, we may write, for Mode I,

$$\sigma_{ij} = \frac{K_1}{(2\pi r)^{\frac{1}{2}}} f_{ij}(\theta) + \sigma_{ij}^{\circ} \qquad (i.j. = n, z)$$

$$(II.1)$$

where:

σ_{ij} are components of stress

K_1 is SIF

r, θ are measured from crack tip (Fig. II-1)

σ_{ij}° are non-singular stress components.

Then, along $\theta = \pi/2$, after truncating σ_{ij}

$$(\tau_{nz})_{max} = \frac{K_1}{(8\pi r)^{\frac{1}{2}}} + \tau^{\circ} = \frac{K_{AP}}{(8\pi r)^{\frac{1}{2}}} \qquad (II.2)$$

where $\tau^{\circ} = f(\sigma_{ij}^{\circ})$ and is constant over the data range

K_{AP} = apparent SIF

τ_{nz} = maximum shear stress in nz plane

$$\therefore \frac{K_{AP}}{\bar{\sigma}(\pi a)^{\frac{1}{2}}} = \frac{K_1}{\bar{\sigma}(\pi a)^{\frac{1}{2}}} + \frac{\sqrt{8}\tau^{\circ}}{\bar{\sigma}} \left(\frac{r}{a}\right)^{\frac{1}{2}} \qquad (II.3)$$

where (Fig. II.1) a = crack length, and $\bar{\sigma}$ = remote normal stress

i.e. $\frac{K_{AP}}{\bar{\sigma}(\pi a)^{\frac{1}{2}}}$ vs. $\sqrt{\frac{r}{a}}$ is linear.

Since from the Stress-Optic Law

$(\tau_{nz})_{max} = \frac{nf}{2t}$ where

n = stress fringe order

f = material fringe value

t = specimen (or slice) thickness

and from Eq. II.2

$$K_{Ap} = (\tau_{nz})_{max}(8\pi r)^{\frac{1}{2}} = \frac{nf}{2t}(8\pi r)^{\frac{1}{2}},$$

then K_{Ap} (through a measure of n) and r become the measured quantities from the stress fringe pattern at different points in the pattern.

A typical plot of normalized K_{AP} vs. $\sqrt{r/a}$ for a homogeneous specimen is shown in Fig. II.2.

Mixed Mode Algorithm

The mixed mode algorithm was developed (see Fig. II-3) by requiring that:

$$\lim_{\substack{r \to o \\ \Theta_m \to \Theta_m^c}} \left\{ (8\pi r_m)^{1/2} \frac{\delta(\tau)_{nz}^{max}}{\delta\Theta} (K_1, K_2, r_m, \Theta_m, \tau_{ij}) \right\} = 0 \tag{II.4}$$

which leads to:

$$\left(\frac{K_2}{K_1}\right)^2 - \frac{4}{3}\left(\frac{K_2}{K_1}\right) cot2\Theta_m^c - \frac{1}{3} = 0 - - - \tag{II.5}$$

By measuring Θ_m^c which is approximately in the direction of the applied load, K_2/K_1 can be determined.

Then writing:

$$\tau_{nz}^{max} = \frac{fn}{2t} = \frac{K_{AP}^*}{(8\pi r)^{\frac{1}{2}}}$$

one may plot $\frac{K_{AP}^*}{\delta(\pi a)^{\frac{1}{2}}}$ vs. $\sqrt{r/a}$ as before, locate a linear zone and extrapolate to $r = o$ to obtain K^*. Knowing, K^*, K_2/K_1 and Θ_m^c, values of K_1 and K_2 may be determined since.

$$K^* = [(K_1 sin\Theta_m^c + 2K_2 cos\Theta_m^0)^2 + (K_2 sin\Theta_m^c)^2]^{\frac{1}{2}} - - - \tag{II.6}$$

Details are found in (Smith and Kobayashi, 1993). A plot of $K_{AP}^*/\sigma\sqrt{\pi/a}$ vs. $\sqrt{r/a}$ will yield a linear zone from which K^* can be extracted. Knowing K^* and θ_m^c, K_1 & K_2 can be determined from Eqs. II.5 and II.6.
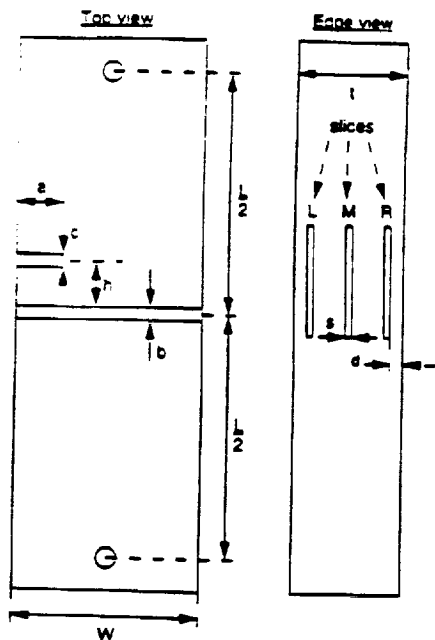
Fig. 1 Specimen Dimensions
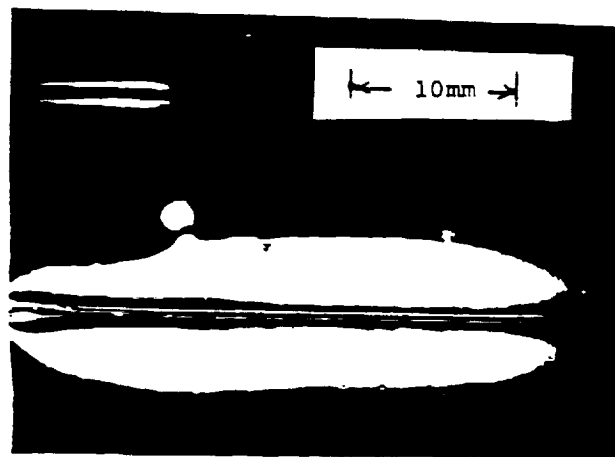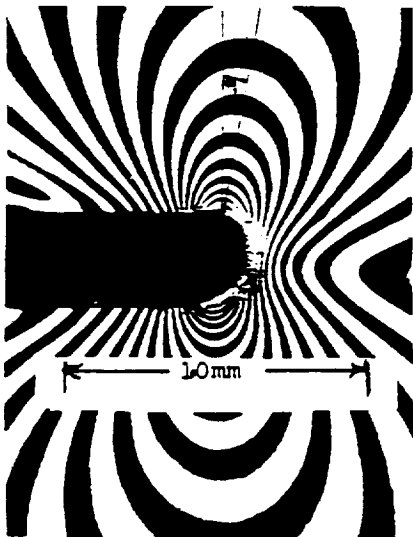B-1, B-2, B-3 Homogeneous Bonded
B-4, B-5,B-6 Bimaterial Bonded

Fig. 2 B-1 ($h = 12.7mm$) No Load Photo After Stress Freezing Cycle (Data zone lies between 1.17 and 3.43 mm above crack tip⊥ to crack plane for B-1, B-2 and B-3)

Fig. 3 (a)TT Loaded Fringe Pattern for B-3(b) Middle Slice Fringe Pattern for B-3

Fig. 4 No-Load Fringe Pattern for B-4 (12.7mm) Data Zone lies between 1.17 and 3.43 mm above crack tip along a reading line inclined 8° to a normal to the crack plane for B-4, 13° for B-5 and 17° for B-6.

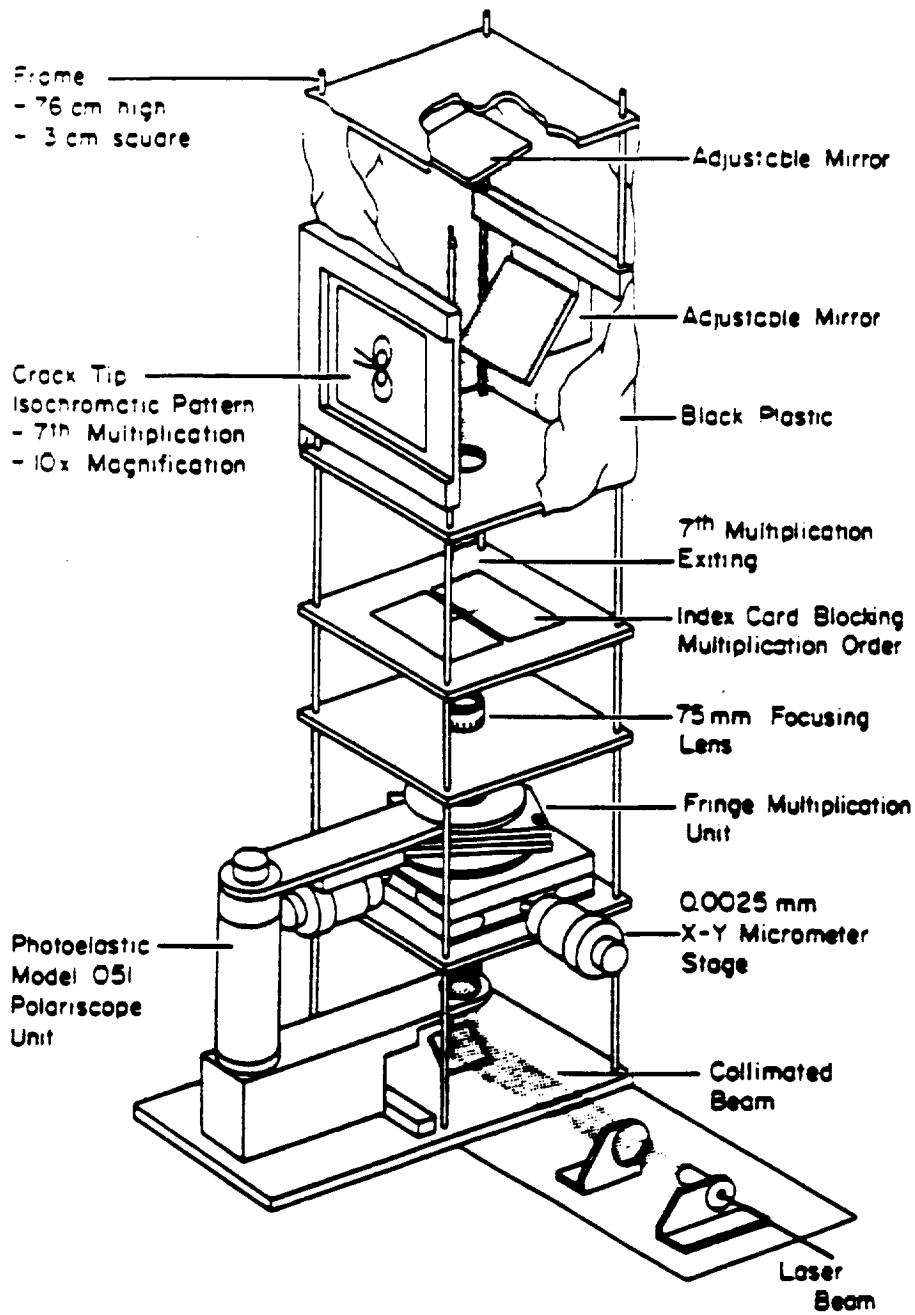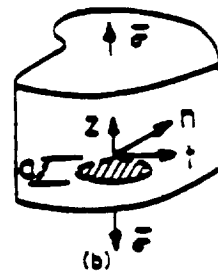← Fig. 5 Near Tip TT Fringe Pattern for B-4 (12.7mm)

Frame
- 76 cm high
- 3 cm square

Adjustable Mirror

Adjustable Mirror

Crack Tip
Isochromatic Pattern
- 7th Multiplication
- 10x Magnification

Black Plastic

7th Multiplication
Exiting

Index Card Blocking
Multiplication Order

75 mm Focusing
Lens

Fringe Multiplication
Unit

0.0025 mm
X-Y Micrometer
Stage

Photoelastic
Model 051
Polariscope
Unit

Collimated
Beam

Laser
Beam

Fig. I-1 Refined Polariscope

(a)

(b)

Fig. II-1 Mode 1
Near Tip Notation
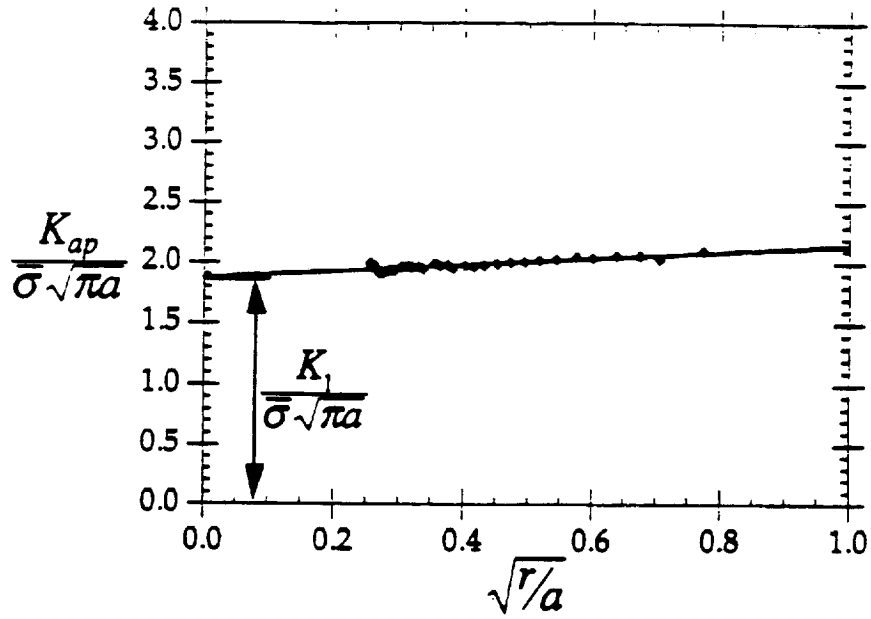
Figure II-2: Middle Slice Data (B-3)
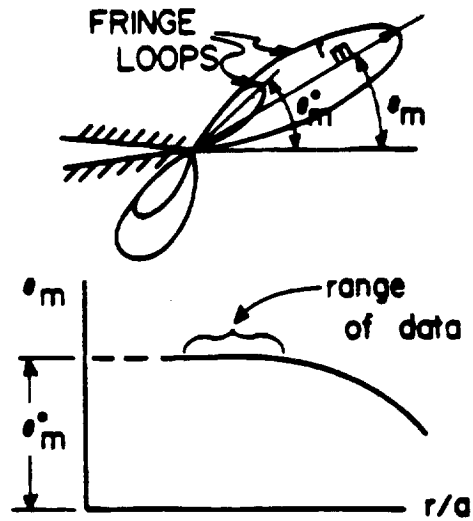
Fig. II-3 Determination of Θ_m° for Mixed Mode Case